

Evaluation of Semiempirical Atmospheric Density Models for Orbit Determination Applications*

C. M. Cox, R. J. Feiertag, and D. H. Oza
Computer Sciences Corporation (CSC)
Lanham-Seabrook, Maryland, USA

C. E. Doll
National Aeronautics and Space Administration (NASA)
Goddard Space Flight Center (GSFC)
Greenbelt, Maryland, USA

Abstract

This paper presents the results of an investigation of the orbit determination performance of the Jacchia-Roberts (JR), Mass-Spectrometer-Incoherent-Scatter-1986 (MSIS-86), and Drag-Temperature-Model (DTM) atmospheric density models. Evaluation of the models was performed to assess the modeling of the total atmospheric density. This study was made generic by using six spacecraft and selecting time periods of study representative of all portions of the 11-year solar cycle. Performance of the models was measured for multiple spacecraft, representing a selection of orbit geometries from near-equatorial to polar inclinations and altitudes from 400 kilometers to 900 kilometers. The orbit geometries represent typical low Earth-orbiting spacecraft supported by the Goddard Space Flight Center (GSFC) Flight Dynamics Division (FDD).

The best available modeling and orbit determination techniques using the Goddard Trajectory Determination System (GTDS) were employed to minimize the effects of modeling errors. The latest geopotential model available during the analysis, the Goddard Earth Model-T3 (GEM-T3), was employed to minimize geopotential model error effects on the drag estimation. Improved-accuracy techniques identified for TOPEX/Poseidon orbit determination analysis were used to improve the Tracking and Data Relay Satellite System (TDRSS)-based orbit determination used for most of the spacecraft chosen for this analysis.

This paper shows that during periods of relatively quiet solar flux and geomagnetic activity near the solar minimum, the choice of atmospheric density model used for orbit determination is relatively inconsequential. During typical solar flux conditions near the solar maximum, the differences between the JR, DTM, and MSIS-86 models begin to become apparent. Time periods of extreme solar activity, those in which the daily and 81-day mean solar flux are high and change rapidly, result in significant differences between the models. During periods of high geomagnetic activity, the standard JR model was outperformed by DTM. Modification of the JR model to use a geomagnetic heating delay of 3 hours, as used in DTM, instead of the 6.7-hour delay produced results comparable to or better than the DTM performance, reducing definitive orbit solution ephemeris overlap differences by 30 to 50 percent. The reduction in the overlap differences would be useful for mitigating the impact of geomagnetic storms on orbit prediction.

1.0 Introduction

Orbit determination for spacecraft whose perigee heights are less than 2000 kilometers (km) requires a comprehensive atmospheric density model because atmospheric drag effects exert significant perturbation forces on spacecraft at these altitudes. Currently, the Goddard Trajectory Determination System (GTDS) provides the user with two atmospheric density models. One model is the Jacchia 1970 model (Reference 1) with analytical modifications given by Roberts (Reference 2), also referred to as the Jacchia-Roberts (JR) model. The JR model was updated to reflect the Jacchia 1971 model constants (Reference 3). The other model is the modified Harris-Priester (HP) model (Reference 4). At the current time, the JR model is used operationally by the Goddard Space Flight Center (GSFC) Flight Dynamics Division (FDD).

Over the past few years, other atmospheric density models, notably the Drag-Temperature Model (DTM) (Reference 5) and the Mass-Spectrometer-Incoherent-Scatter-1986 (MSIS-86) (Reference 6) atmospheric density model, have been constructed based on data unavailable to the JR and HP models and were expected to perform better under

* This work was supported by the National Aeronautics and Space Administration (NASA)/Goddard Space Flight Center (GSFC), Greenbelt, Maryland, under Contract NAS 5-31500.

varying conditions of solar, geomagnetic, and seasonal-variational activity. It is of interest to evaluate these atmospheric models to determine their potential roles in supporting orbit determination efforts in the GSFC Flight Dynamics Facility (FDF), particularly in future mission planning. It was also desirable to test these models in GTDS where an evaluation of model performance could be ascertained by trending of the GTDS solution fit parameters, such as weighted root-mean-square (WRMS) residuals, estimated drag correction factors, and definitive ephemeris overlap comparisons, under various solar and geomagnetic conditions, orbit geometries, and spacecraft area and ballistic coefficients.

1.1 Overview

GTDS is used for current operational orbit determination support by the GSFC FDD. GTDS employs a batch-least-squares algorithm which estimates the set of orbital elements, force modeling parameters, and measurement-related parameters that minimizes the sum of the squared differences between observed and calculated values of selected tracking data measurements over a solution arc (Reference 7). Of interest for this study is the ability of GTDS to estimate a drag scaling parameter ρ_1 , defined by

$$\vec{F}_D = -\frac{1}{2} C_D \rho \vec{V} |\vec{V}| A (1 + \rho_1)$$

where

- ρ = density of atmosphere surrounding the spacecraft
- ρ_1 = drag scaling parameter, here assumed to be a constant
- C_D = coefficient of drag
- A = cross-sectional area of spacecraft
- V = velocity of spacecraft relative to local atmosphere

Assuming that the solar flux and geomagnetic index (GMI) input values are correct and that the ballistic coefficient is calibrated, then the estimated ρ_1 values should be near zero if the model correctly accounts for the density. The density model that yields the smallest average ρ_1 value would generally be assumed to be the most accurate model. A model that accurately describes the density magnitudes and variations over any given set of solutions should result in minimal definitive ephemeris overlap comparisons. Higher overlap comparison values would represent poorer model performance. Also, if a model accurately describes the density magnitudes and variations over any given set of solutions, then the WRMS values of the solutions should be reduced for each spacecraft. Higher WRMS values for each individual spacecraft would represent poorer model performance. Finally, all results were scrutinized for consistency with the predicted model behavior as determined from comparisons of the densities produced by the models.

1.2 Summary of the Models

Atmospheric models are formulated using theoretical and semiempirical methods to obtain equations interrelating the properties of the atmosphere. As accuracy requirements increase, greater reliance is placed on empirical techniques. Dynamic models, also called time-varying models, attempt to predict the structure of the atmosphere in space and time as the atmosphere responds to varying conditions. Changing atmospheric structure is attributable to solar, geomagnetic, diurnal, semiannual, seasonal-latitudinal, and unpredicted day-to-day variations (Reference 8).

The era of semiempirical models began with the Jacchia 1965 model (Reference 9), a dynamic model, where the prime data were derived from atmospheric drag on satellites. Although the Jacchia model was built around a static model derived by integration of the diffusion equations, thermospheric variations were introduced by use of empirical formulas. The MSIS series of models began with the analysis of atmospheric composition data from the mass spectrometer onboard the Orbital Geophysical Observatory-6 (OGO-6) and a comparison of these data with data derived from a ground-based radar incoherent scattering technique. The MSIS-77 model (Reference 10) eventually gave rise to both the MSIS-86 and DTM models. All are based on the Bates type of analytic temperature profile with boundary conditions on temperature and composition given by spherical harmonic expansions that have been fit to in situ measurements. Table 1 summarizes some major features of the models evaluated here.

Table 1. Features of the JR, MSIS-86, and DTM Models

Model Features	Jacchia-Roberts (Updated to Jacchia 1971 Standard)	MSIS-86	DTM
Variations with solar flux	Daily and 81-day centered average	Daily and 81-day centered average	Daily and 81-day centered average
Geomagnetic heating delay	6.7 hours	0-59 hours, with local variations	3 hours
Density for each constituent gas	Only for total	Yes	Yes
Local variations in density	No	Yes, by constituents	Yes, by constituents
Diurnal variations	Yes	Yes, by constituents	Yes, by constituents
Semiannual variation	Yes	Yes, by constituents	Yes, by constituents
Seasonal latitudinal variations of lower thermosphere boundary	Limited to heights from 90-120 km	Yes, expressed as spherical harmonics	Yes, expressed as spherical harmonics
Seasonal latitudinal variations of helium	Yes	Yes	Yes
Hydrogen effects (important above 1200 km)	No	Yes	Yes

In general, the best data coverage is in the 150-km to 600-km range. Jacchia does have some data from higher altitudes; however, in general, reliable data outside this range are very sparse, and density extrapolations based on several assumptions become increasingly inaccurate for all models as altitudes vary from this region.

1.3 Direct Comparison of the Models

Atmospheric densities predicted by the JR, HP, and MSIS-86 models at various altitudes for common input values of solar and geomagnetic activity were compared for June 22, 1992. The solar activity is characterized by the 10.7-centimeter solar flux, designated in this paper as $F_{10.7}$ (with implied units of 10^{-22} watts per meter² per hertz). The geomagnetic activity is characterized by the K_p and A_p geomagnetic indices (unitless, where K_p values are expressed in a logarithmic scale and A_p values are expressed in a linear scale). Analysis (Reference 11) revealed that the local atmospheric density variations between the MSIS-86 and JR models ranged between -40 percent and +80 percent for low solar activity ($F_{10.7} = 100$, $K_p = 2$) and between -40 percent and +40 percent for high solar activity ($F_{10.7} = 200$, $K_p = 2$). These differences represent many subtle differences among the models, the most significant local variation being in the behavior of the diurnal bulge. As altitudes increase, the diurnal bulge movement is generally southward and is primarily related to the seasonal-latitudinal helium effect, which generally dominates at altitudes above 500 km, where helium flows toward the winter pole.

Differences between static global averages of densities produced by the JR and MSIS-86 models are less than 15 percent during low solar activity time periods ($F_{10.7} = 100$, $K_p = 2$). The differences are most pronounced for the averages representing polar orbits, where values just under 25 percent were observed. At higher solar flux values ($F_{10.7} = 200$, $K_p = 2$) and altitudes above 400 km, MSIS-86 predicts smaller densities than JR. Increasing GMI ($F_{10.7} = 200$, $K_p = 5$) results in a similar effect.

Average density plots as a function of time (for altitudes of 300 km, 700 km, and 1300 km) show marked differences between the models, particularly in response to GMI fluctuations. The JR model employs a single K_p value 6.7 hours prior to the current time, whereas the MSIS-86 model employs 21 3-hour A_p values spanning 59 hours prior to the desired time. Comparison of the time-dependent densities reveal that MSIS-86 and JR are similar in density magnitude in the lower and middle altitudes for moderate GMI activity but tend to have the strongest reactions to high GMI activity in the middle to high altitudes. At high altitudes, JR densities are always greater than MSIS-86 densities due to a spiking effect in JR, where the tendency is for JR to exhibit a rapid and large peak density spike and for MSIS-86 to display a broad-based spike. The timing of the MSIS-86 density peak precedes the JR peak by approximately 6 hours. In general, the JR model response to solar and geomagnetic activity was greater than that of the MSIS-86 model. Overall, the largest difference in the models was in their reaction to high GMI activity conditions, although their reactions to the solar flux also differed. The large differences observed in the densities produced by the different models can have a significant effect on areas such as mission planning, where the density is important in determining orbit decay rates.



Table 4. Parameters and Options Used in the GTDS Solutions

Orbit Determination Parameter or Option	User Spacecraft	TDRS
Estimated parameters	Orbital state, ρ_1 , and station measurement biases (USO bias and drift, COBE only)	Orbital state, coefficient of solar radiation pressure (C_R), BRTS range bias
Integration type	Cowell 12th order	Cowell 12th order
Coordinate system of integration	Mean of J2000.0	Mean of J2000.0
Integration step size (seconds)	60 seconds	600 seconds
Tracking measurements	TDRSS two-way Doppler (TD2S) TDRSS two-way range (TR2S) TDRSS one-way Doppler (TD1S) Ground S-band range rate (URDF)	BRTS two-way range
Data span	2 days (4 for COBE)	See text
Data rate	1 per 10 seconds	1 per 10 seconds
Editing criterion	3σ Central angle to local horizon	3σ
Measurement weight sigmas	TD2S: 0.25 hertz TR2S: 30 meters TD1S: 0.13 hertz URDF: 10 centimeters/second	10 meters
Satellite area model (all constant)	COBE: 17.8 meters ² ERBS: 4.7 meters ² HST: 74.0 meters ² LA4: 12.3 meters ² LA5: 12.7 meters ² SMM: 17.5 meters ²	40 meters ²
Satellite mass	COBE: 2155.00 kilograms ERBS: 2116.00 kilograms HST: 11328.00 kilograms LA4: 1900.32 kilograms LA5: 1913.25 kilograms SMM: 2315.59 kilograms	TDRS-4 ~ 1900 kilograms TDRS-3 ~ 1990 kilograms TDRS-1 ~ 1730 kilograms
Geopotential model	50 x 50 GEM-T3	20 x 20 GEM-T3
Atmospheric density model	JR, MSIS-86, DTM	N/A
Solar and lunar ephemerides	DE 200	DE 200
Coefficient of drag (C_D)	2.2 (2.3 for COBE)	N/A
User-spacecraft antenna offset	Constant radial	No
Tropospheric refraction correction	Yes	Yes
Ionospheric refraction correction		
Ground-to-spacecraft	Yes	Yes
Spacecraft-to-spacecraft	No (central angle edit instead)	N/A
Polar motion correction	Yes	Yes
Solid Earth tides	Yes	Yes

NOTE: GEM = Goddard Earth Model
DE = Developmental Ephemeris
LA = Landsat
N/A = not applicable
URDF = unified S-band range differencing
USO = ultrastable oscillator



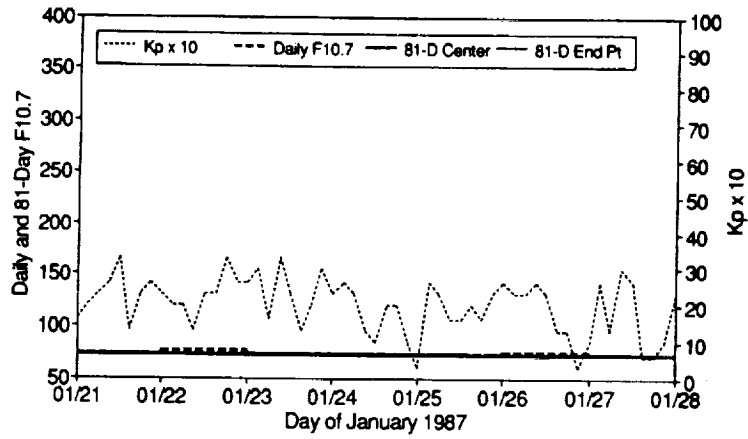


Figure 1. Solar Flux and GMI for Period A

Table 5. Summary of Orbit Determination Solution Results for Period A

Spacecraft	Density Model	ρ_1	WRMS	Overlap MPD (meters)
ERBS	JR	-0.01 ± 0.22	0.21 ± 0.04	23.5 ± 6.6
	MSIS-86	-0.07 ± 0.25	0.21 ± 0.04	23.5 ± 6.6
	DTM	-0.24 ± 0.18	0.21 ± 0.04	23.5 ± 6.6
Landsat-5	JR	-0.01 ± 0.31	0.21 ± 0.05	27.7 ± 10.9
	MSIS-86	-0.01 ± 0.31	0.21 ± 0.05	27.3 ± 10.3
	DTM	-0.16 ± 0.26	0.21 ± 0.05	27.3 ± 10.5
SMM	JR	-0.27 ± 0.04	0.26 ± 0.03	26.7 ± 7.8
	MSIS-86	-0.14 ± 0.03	0.24 ± 0.02	23.9 ± 9.2
	DTM	-0.37 ± 0.02	0.25 ± 0.02	24.6 ± 9.3

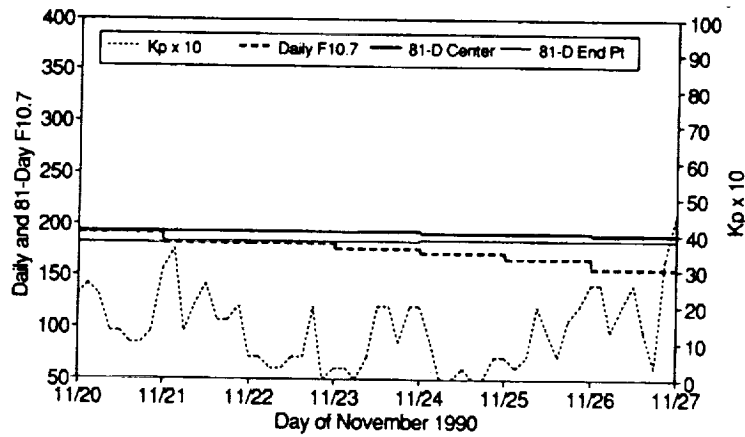


Figure 2. Solar Flux and GMI for Period B

PRECEDING **MISSING PAGES** NOT FILMED

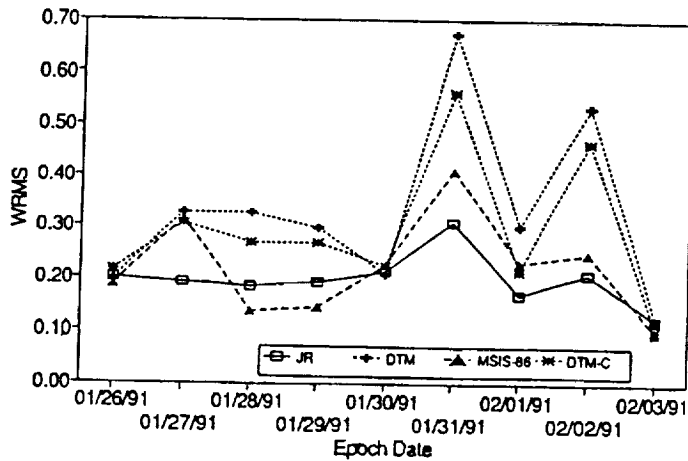


Figure 6. ERBS Solution WRMS Results for Period C

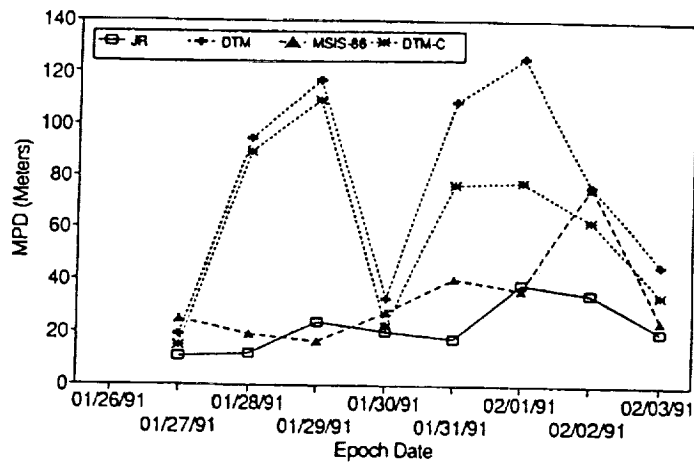


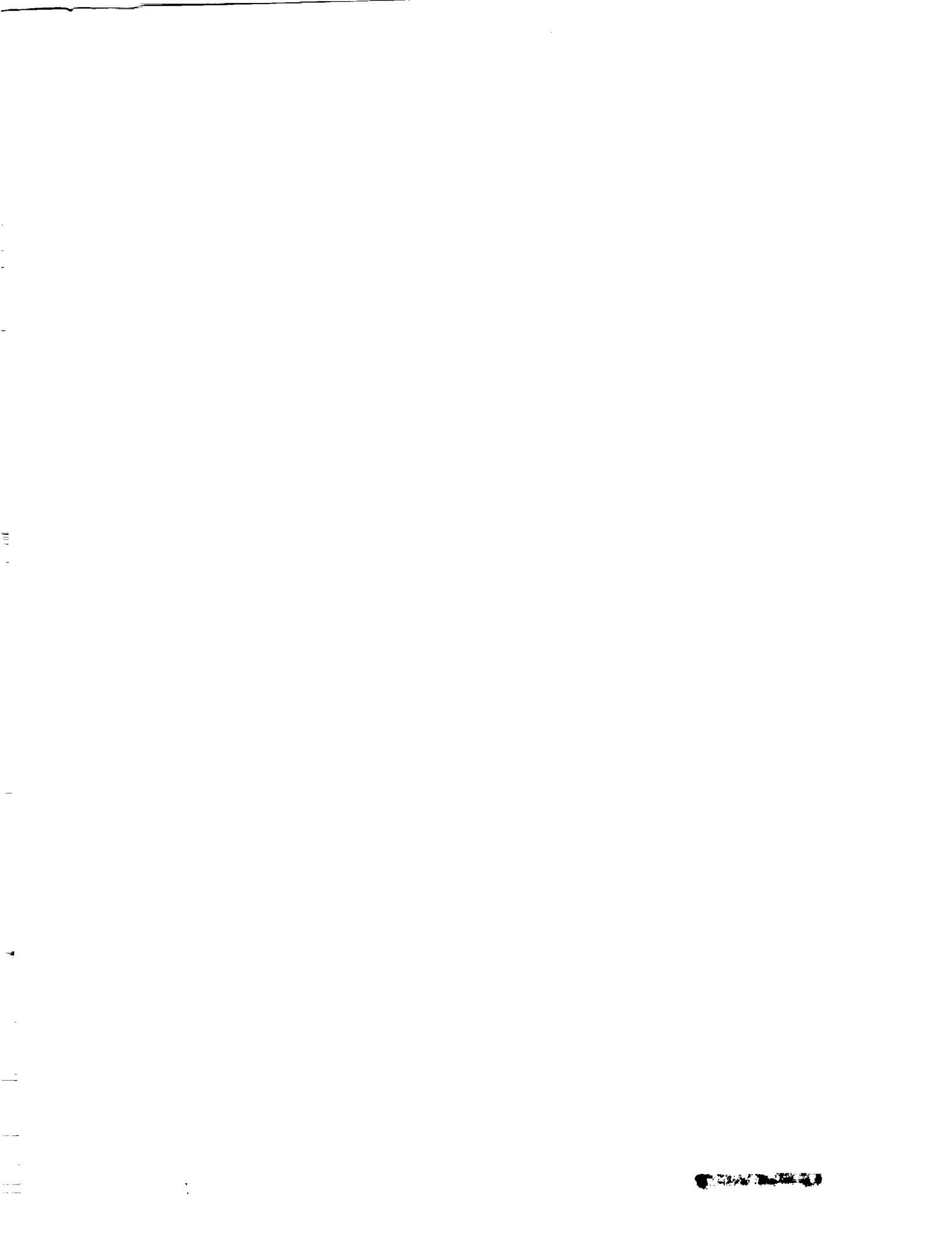
Figure 7. ERBS Solution Overlap MPD Results for Period C

Table 7. Summary of Orbit Determination Solution Results for Period C

Spacecraft	Density Model	ρ_1	WRMS	Overlap MPD (meters)
COBE	JR	-0.21 ± 0.04	0.22 ± 0.02	30.4 ± 12.4
	MSIS-86	-0.01 ± 0.06	0.23 ± 0.01	41.8 ± 17.2
	DTM	-0.82 ± 0.34	0.36 ± 0.07	103.4 ± 34.1
	DTM-C	-0.14 ± 0.15	0.32 ± 0.04	82.4 ± 21.8
ERBS	JR	-0.08 ± 0.05	0.20 ± 0.05	22.4 ± 9.3
	MSIS-86	-0.04 ± 0.08	0.22 ± 0.09	33.3 ± 17.7
	DTM	-0.50 ± 0.38	0.33 ± 0.16	77.6 ± 37.9
	DTM-C	-0.07 ± 0.18	0.29 ± 0.13	61.2 ± 31.6
HST	JR	-0.24 ± 0.05	0.28 ± 0.10	39.6 ± 24.0
	MSIS-86	-0.13 ± 0.05	0.28 ± 0.09	50.8 ± 36.6
	DTM	-0.27 ± 0.26	0.55 ± 0.31	115.5 ± 84.5
	DTM-C	-0.20 ± 0.12	0.45 ± 0.24	85.1 ± 70.3
Landsat-4	JR	-0.23 ± 0.04	0.17 ± 0.09	21.5 ± 7.9
	MSIS-86	-0.00 ± 0.10	0.19 ± 0.10	37.9 ± 23.9
	DTM	-0.60 ± 0.42	0.26 ± 0.15	87.4 ± 45.4
	DTM-C	-0.03 ± 0.20	0.24 ± 0.12	69.3 ± 32.2

1

MISSING PAGES



Overall, the JR and MSIS-86 models were comparable in performance, while both versions of the DTM model resulted in the worst WRMS and overlap MPD values, on average. All the models had some difficulty with the GMI activity on February 1. Ranked best to worst were JR, MSIS-86, the modified DTM, and the implemented DTM. For all models, the peak solar flux time period is the worst; however, both DTM versions produced overlap differences greater than 200 m (the mission requirement) for HST near the GMI activity on February 1 (see Figure 8).

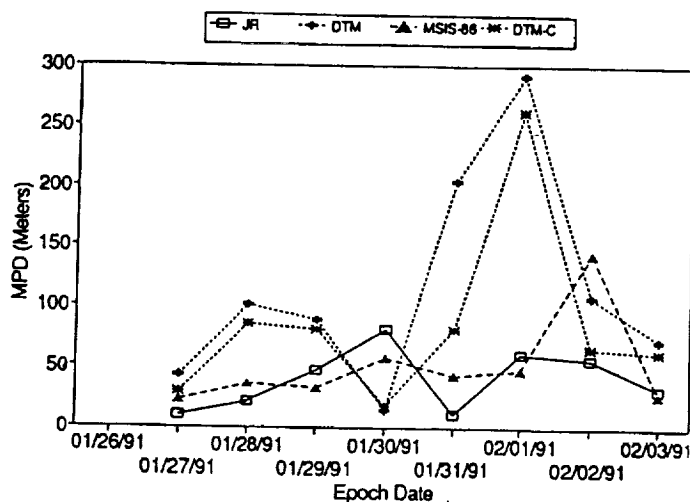


Figure 8. HST Solution Overlap MDP Results for Period C

The ρ_1 values resulting from the originally implemented DTM model based on the 81-day endpoint average solar flux are significantly higher than the JR and MSIS-86 ρ_1 values, while the modified DTM model using the 81-day centered average solar flux resulted in an average ρ_1 comparable to JR and MSIS-86. Daily trends for the solved-for JR and MSIS-86 ρ_1 values are nearly constant. The DTM ρ_1 values start near 0, peak at approximately 0.7 for HST (higher for the other spacecraft), and then return to the -0.2 to 0.2 range. The modified DTM model showed a similar peak; however, the relative height of the peak from the base was only half that seen in the implemented model. The atmospheric density modeled by the DTM model was consistently low during the peak in the daily solar flux activity, as indicated by the ρ_1 trends in both of the DTM cases. This is consistent with a situation in which a portion of the daily solar flux is applied as a daily difference from the mean, as opposed to being correctly applied as part of the mean value. The mean solar flux has a greater effect on the resulting density than the daily contribution. During this time period, the use of an 81-day endpoint-averaged $F_{10.7}$ value will result in a significant portion of the solar flux during the peak activity being applied as the daily solar flux input, resulting in a lower density. The fact that the phenomenon is still apparent with the modified DTM indicates that the DTM model may not handle extreme solar flux input values as well as the JR or MSIS-86 models.

3.4 Period D: Effects of Geomagnetic Activity

Period D was chosen from a time period in which the daily and average solar flux values were behaving in the nominal 27-day period pattern, as in period B, but also included extremely high geomagnetic activity. As shown in Figure 9, the average solar flux was approximately 200, while the daily value was approximately 240, near the maximum of the current 27-day solar rotation. In general, GMI activity was very high, with K_p actually reaching 8.7 (9.3 is the nominal maximum on the logarithmic K_p scale) on one occasion. The behavior of the atmospheric models during such geomagnetic storms is important because the ability or inability to accurately model GMI activity effects can affect the orbit determination and prediction process adversely, as has been observed during the operational and TDRSS Onboard Navigation System (TONS) experiment use of the JR model (Reference 13).

Based on the generally good performance of the DTM model during this period, a second set of results was generated for the JR model; in this case, the delay in the geomagnetic activity was modified from the original 6.7 hours to

3 hours. This change was made based on previous analysis of the performance of the models (Reference 11), which showed JR to have the longest delay in GMI, and because the value Jacchia applied in the original model was an assumed value meant to reflect an average time for the geomagnetic heating effect (Reference 3). The modified JR model is referred to as the JR-3 model in this paper.

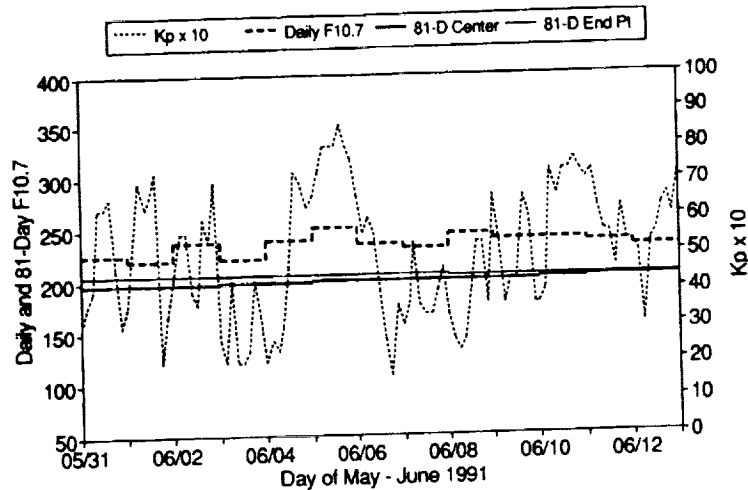


Figure 9. Solar Flux and GMI for Period D

As is evident from Table 8, there were significant variations in the ρ_1 values. The ρ_1 values resulting from the original JR and the modified JR models are comparable. The relatively large negative ρ_1 indicates that the DTM model produced an average density that was too high. The daily trends in the solved-for ρ_1 values, shown in Figure 10 for the ERBS spacecraft, are more active than for other periods, due to the geomagnetic activity. In this case, the MSIS-86 model appears to produce a consistently lower average density than either JR or DTM for those spacecraft that are under 700 km.

Table 8. Summary of Orbit Determination Solution Results for Period D

Spacecraft	Density Model	ρ_1	WRMS	Overlap MPD (meters)
COBE	JR	-0.28 ± 0.06	0.25 ± 0.05	49.1 ± 19.6
	JR-3	-0.28 ± 0.04	0.23 ± 0.02	30.9 ± 11.5
	MSIS-86	-0.18 ± 0.06	0.20 ± 0.02	28.0 ± 6.6
	DTM	-0.16 ± 0.06	0.21 ± 0.01	19.1 ± 5.9
ERBS	JR	-0.21 ± 0.10	0.22 ± 0.08	58.7 ± 56.4
	JR-3	-0.20 ± 0.06	0.20 ± 0.04	33.0 ± 27.2
	MSIS-86	-0.06 ± 0.09	0.23 ± 0.08	53.3 ± 43.2
	DTM	-0.27 ± 0.06	0.22 ± 0.06	35.8 ± 31.5
HST	JR	-0.37 ± 0.09	0.55 ± 0.19	62.9 ± 47.0
	JR-3	-0.38 ± 0.07	0.45 ± 0.28	49.8 ± 26.3
	MSIS-86	-0.27 ± 0.09	0.50 ± 0.25	77.4 ± 60.5
	DTM	-0.52 ± 0.05	0.35 ± 0.24	51.2 ± 26.8
Landsat-4	JR	-0.29 ± 0.10	0.18 ± 0.05	36.2 ± 13.2
	JR-3	-0.38 ± 0.07	0.16 ± 0.04	31.1 ± 22.2
	MSIS-86	-0.16 ± 0.15	0.17 ± 0.03	37.5 ± 25.7
	DTM	-0.29 ± 0.06	0.17 ± 0.04	33.4 ± 19.4

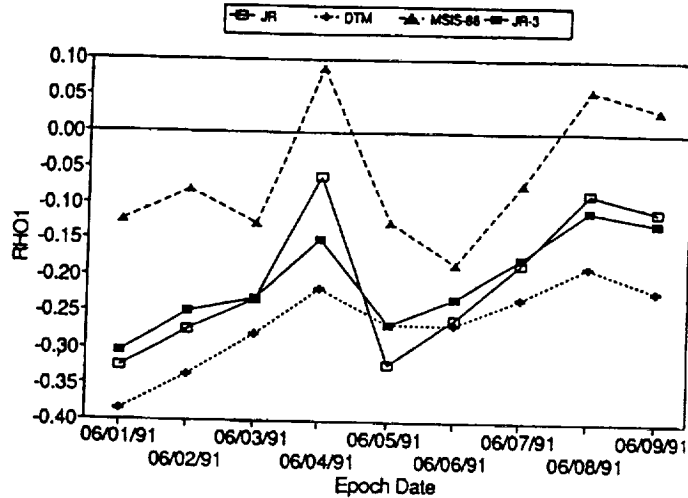


Figure 10. ERBS Solution ρ_1 Results for Period D

The increased WRMS and MPD values during the GMI storm on June 4 through June 7 show that there was sensitivity to the GMI, especially for the models with the longer delay in GMI modeling (JR and MSIS-86). Solution WRMS values showed significant variations between the models and were adversely affected by the GMI activity during this period. Surprisingly, the COBE WRMS values from the DTM model were little affected by the change in GMI activity on June 6 and June 9, unlike the JR and MSIS-86 models, both of which showed increased WRMS values. The modified JR produced individual solution WRMS values similar in trend to DTM.

For all models the worst overlaps are seen at the onset and ends of the large storm from June 5 through June 9. The unmodified JR and MSIS-86 models produced overlaps of approximately 175 meters in the 2σ to 3σ range. The JR-3 MPDs are generally improved over the standard JR model. The Landsat-4 overlap values are significantly lower than the HST and ERBS MPD values for this period due to the absence of the overlap for the June 4 and June 5 solutions because of an orbit maintenance maneuver. This period shows an improvement when the JR-3 model is used instead of the standard JR model; however, it is not clear that it is the best performer when compared with DTM and MSIS 86.

3.5 Long-Term Changes in Density Model Performance

The long-term behavior of the estimated ρ_1 values is of interest because it indicates long-term variations in the modeling of the atmospheric density. To do this accurately, it is necessary to consider the ρ_1 values for those spacecraft for which the ballistic coefficient remained constant. In this study the only spacecraft that fit this requirement are ERBS and COBE. Figure 11 illustrates the average ρ_1 values (Rho1 in Figure 11) for each model used in the ERBS orbit solutions. (JR-3 applies to period D only, while DTM-C applies to period C only). The ρ_1 values for both the JR and MSIS-86 models change significantly depending on the study period. The total range of the JR ρ_1 is from approximately 0 to -0.4, representing up to 67 percent of the actual atmospheric density. DTM varies also, but the total range is somewhat smaller assuming that the DTM using the 81-day centered average solar flux is the correct implementation (for Period C). COBE does not exhibit as wide a range of change in the average ρ_1 , but the average changes by up to 0.3 for DTM. Overall, the change in the average ρ_1 indicates that calibrating the ballistic coefficient for use in long-term ephemeris propagations will need to be a routine process with regular updates. Failure to update the ballistic coefficient periodically will result in propagation errors because there would be no accounting for long-term errors in the atmospheric models.

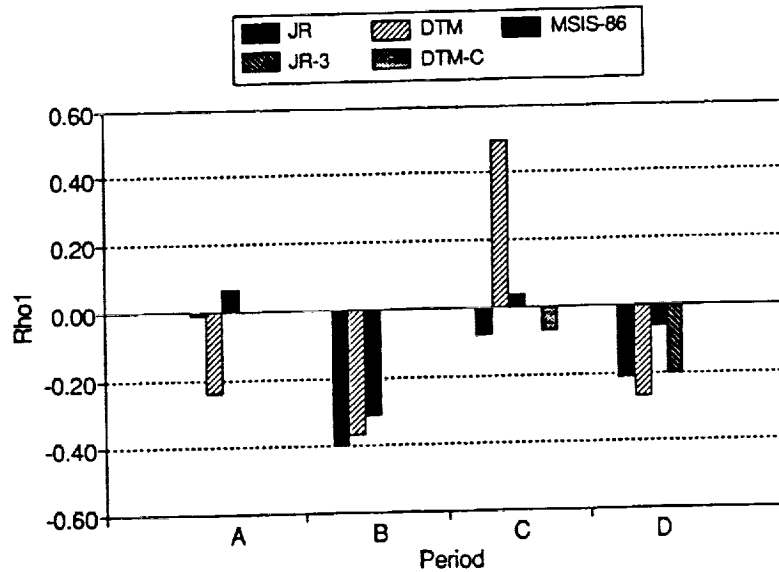


Figure 11. ERBS Long-Term Solution ρ_1 Changes

4.0 Summary and Conclusions

Performance of the three atmospheric density models was measured for multiple spacecraft, representing a selection of orbit geometries from near-equatorial to polar inclination; altitudes from 400 km to 900 km; and inclinations of 28, 57, and 99 degrees. The orbit geometries chosen represent typical low Earth-orbiting spacecraft supported by the GSFC FDD.

Overall, evaluation of the relative performance of the atmospheric models was based primarily on the solution overlap maximum position differences. The solution WRMS values showed less difference between the models, indicating that the relative level of error in the orbit solutions is still high compared with the relative level of improvement between the models. However, in some instances there was significant change in the solution WRMS values. In most cases, the WRMS values and the overlap MPDs result in similar conclusions.

During periods of relatively quiet $F_{10.7}$ activity near the solar minimum, without extreme geomagnetic activity, the choice of atmospheric density model is relatively inconsequential. During typical solar flux conditions near the solar maximum, the differences between the JR, DTM, and MSIS-86 models begin to become apparent, with JR providing marginally improved results. Time periods of extreme solar activity, i.e., those in which the daily and 81-day mean solar flux are high ($F_{10.7}$ greater than 270+) and changing rapidly, result in significant differences between the models. Generally, the JR model performed the best, while DTM performed the worst.

The choice of an 81-day centered average solar flux for use in the DTM model resulted in substantial improvement in performance. This demonstrates that the 81-day centered average solar flux should be used as specified in the original paper for optimal model performance. However, the improvements in the DTM performance resulting from this change were not enough for the model to outperform the JR model.

Geomagnetic activity produced the largest differences in performance of the models. The analysis results show that the standard JR model, which has a 6.7-hour delay for geomagnetic effects, was outperformed by DTM, which has a 3-hour delay. Modification of JR to use a 3-hour delay produces results comparable to or better than the DTM performance, with definitive overlaps typically being reduced by 30 to 50 percent. The reduction in the overlap performance, with definitive overlaps typically being reduced by 30 to 50 percent. The reduction in the overlap differences would help mitigate the impact of GMI storms on FDD deliverables. Given that significant GMI activity is present throughout the solar cycle and that the relative contribution of the solar flux to the atmospheric density is greatly reduced during the solar minimum, the ability of an atmospheric density model to accurately reflect the GMI effects is particularly critical.

Under most circumstances, the differences in the orbit determination performances of these models is negligible. Under conditions of unsettled geomagnetic activity, the JR model currently implemented in GTDS did not provide optimal performance. With the exception of COBE, the DTM model appeared to handle GMI activity best for the spacecraft used during that period. Modification of the JR model geomagnetic activity modeling to reflect a 3-hour delay instead of the default 6.7-hour delay produced results that were similar to or marginally better than the DTM results. This modification to the JR model is not in conflict with Jacchia's published works and is further supported by previous FDF analysis (Reference 14)

References

1. Smithsonian Astrophysical Observatory Special Report No. 313, *New Static Models of the Thermosphere and Exosphere With Empirical Temperature Profiles*, L. G. Jacchia, 1970
2. E. R. Roberts, Jr., "An Analytical Model for Upper Atmosphere Densities Based Upon Jacchia's 1970 Models," *Celestial Mechanics*, Vol. 4, No. 3, 1971, pp. 368-377
3. L. G. Jacchia, Smithsonian Astrophysical Observatory Special Report No. 332, *Revised Static Models of the Thermosphere and Exosphere with Empirical Temperature Profile*, May 1971
4. I. Harris and W. Priestler, "Time-Dependent Structure of the Upper Atmosphere," *Journal of the Atmospheric Sciences*, Vol. 19, No. 4, 1962, pp. 286-301
5. F. Barlier, C. Berger, J. L. Falin, G. Kockarts, and G. Thuillier, "A Thermospheric Model Based on Satellite Drag Data," Institut D'Aeronomic Spatiale de Belgique, *Aeronomica Acta*, 1977
6. A. E. Hedin, "The Atmospheric Model in the Region 90 to 2000 km," *Advanced Space Research*, Vol. 8, No. 5-6, 1988, pp. 5(9)-5(25)
7. Goddard Space Flight Center, Flight Dynamics Division, FDD/552-89/001, *Goddard Trajectory Determination System (GTDS) Mathematical Theory, Revision 1*, A. C. Long and J. O. Cappellari, Jr., (CSC) and A. J. Fuchs and C. E. Velez (GSFC) (editors), prepared by Computer Sciences Corporation, July 1989
8. National Oceanic and Atmospheric Administration, Prompt Report No. 515, *Solar-Geophysical Data (Supplement)*, H. E. Coffey, John A. McKinnon (editors), et al., July 1987
9. L. G. Jacchia, "Static Diffusion Models of the Upper Atmosphere With Empirical Temperature Profiles," *Smithsonian Contribution to Astrophysics*, Vol. 8, 1965, pp. 215-257
10. G. Thuillier, J. L. Falin, and F. Barlier, "Global Experiment Model of the Exospheric Temperature Using Optical and Incoherent Scatter Measurements," *Journal of Atmospheric and Terrestrial Physics*, Vol. 39, 1977, p. 1195
11. Goddard Space Flight Center, Flight Dynamics Division, 553-FDD-93/014R0UD0, *Schatten Solar Flux Prediction and Jacchia-Roberts Atmospheric Density Model Analysis*, C. Cox, R. Feiertag, and M. Radomski (CSC), prepared by Computer Sciences Corporation, September 1993
12. Goddard Space Flight Center, Flight Dynamics Division, 553-FDD-93/086R0UD0, *Orbit Determination Performance Analysis of the Jacchia-Roberts, Mass-Spectrometer-Incoherent Scatter-1986, and Drag-Temperature Model Atmospheric Density Models*, C. Cox and R. Feiertag (CSC), prepared by Computer Sciences Corporation, December 1993
13. Goddard Space Flight Center, Flight Dynamics Division, 553-FDD-93/005R0UD0, *Tracking and Data Relay Satellite System (TDRSS) Onboard Navigation System (TONS) Experiment Second Quarter Status Report*, A. Long et al., prepared by Computer Sciences Corporation, March 1993
14. Computer Sciences Corporation, CSC/TM-80/6173, *An Evaluation of the Geomagnetic Activity Effect in the GTDS Jacchia-Roberts Atmospheric Density Model*, T. Lee and K. Willig, September 1980

